



## **Stability assumptions in numerical modeling of cold-formed steel-framed buildings under seismic loading**

Mohammed M. Eladly<sup>1</sup>, Zhidong Zhang<sup>2</sup>, Amanpreet Singh<sup>3</sup>, Jiachen Zhang<sup>4</sup>, Tara C. Hutchinson<sup>5</sup>, Benjamin W. Schafer<sup>6</sup>

### **Abstract**

In the U.S., current seismic provisions limit the height of cold-formed steel (CFS) framing in buildings to six-stories. Utilizing component-level laboratory tests, with strength levels higher than current code-available values, a ten-story CFS-framed building archetype was professionally designed to explore the potential for taller buildings and address the increasing need for resilient, efficient, non-combustible urban residential housing. This year, a series of shake-table tests on a slice of the ten-story archetype building will be conducted at the UC San Diego 6-DOF Large High-Performance Outdoor Shake Table Facility. This archetype building capstone experimental program is part of the NSF-funded collaborative research program: Seismic Resiliency of Repetitively Framed Mid-Rise Cold-Formed Steel Buildings (CFS-NHERI). In preparation for the experimental program, a high-fidelity finite element model of the building has been developed in OpenSeesPy. The model uses a combination of phenomenological and mechanically-driven elements, enriched with findings from prior component and fastening test programs. The nature in which stability is handled in the model has an important impact on the predicted response. This paper presents the assumptions inherent in the model when considering the large variety of geometric nonlinearity that exists, including: buckling of steel sheets; local, distortional, and global buckling of CFS members and story-level P-Delta effects. Predicted response under earthquake loading is presented and compared with results generated by a design-level model. It is intended that the findings of this research can help guide the development of strategies for incorporating stability limits into the seismic modeling of CFS-framed buildings, thereby enhancing the analysis, resilience, and application of these structures.

### **1. Introduction**

Cold-formed steel (CFS) framing systems have become increasingly popular in the North American construction industry, particularly for low-rise and mid-rise buildings. However, current building codes (ASCE/SEI 2016, 2022) impose a height limitation of 19.8 m (65 ft) for CFS-

---

<sup>1</sup> Graduate Research Assistant, Johns Hopkins University, <eladly@jhu.edu>

<sup>2</sup> Postdoctoral Research Associate, University of Virginia, <zz9km@virginia.edu>

<sup>3</sup> Postdoctoral Research Associate, Johns Hopkins University, <amanprs@jhu.edu>

<sup>4</sup> Graduate Research Assistant, University of California San Diego, <j-charlie-zhang@ucsd.edu>

<sup>5</sup> Professor, University of California San Diego, <tahutchinson@ucsd.edu>

<sup>6</sup> Professor, Johns Hopkins University, <schafer@jhu.edu>

framed structures in Seismic Design Category (SDC) C and SDC D regions. While substantial research has been conducted on individual components of CFS buildings, significantly advancing codes and standards such as AISI S100 (2016), S240 (2015a), and S400 (2015b), studies on the system-level performance of CFS structures under seismic loads remain limited. To date, only two projects in North America have examined the seismic behavior of complete CFS systems using large shake tables. The first project, known as the CFS-NEES project, involved shake table testing of a full-scale, two-story CFS-framed building. Conducted by Peterman et al. (2016) at the NEES@Buffalo facility, this was the first study to assess the system-level seismic response of a CFS-framed structure in North America. The two-story building measured 15.2 m x 7 m (49 ft 9 in x 23 ft) in plan. The second project, referred to as the CFS-HUD project, was carried out by Hutchinson et al. (2021) at the NEES@UC San Diego facility. This project included seismic testing and post-earthquake fire testing of a full-scale, six-story mid-rise CFS wall-braced building. The CFS-HUD test building had a floor plan of 10.4 m x 7.3 m (34 ft x 24 ft) with a story height of 3.1 m (10 ft).

The multi-university-industry initiative titled Seismic Resiliency of Repetitively Framed Mid-Rise Cold-Formed Steel Buildings (CFS-NHERI), with primary funding by the National Science Foundation (NSF), was launched to enhance the understanding of the seismic behavior of mid-rise CFS-framed building systems and apply this gained knowledge toward improving seismic design codes for such structures. As part of the CFS-NHERI project, a series of experiments have been conducted to investigate the nonlinear behavior of components and connections. Notable contributions from this research project include studies by Singh et al. (2022b, 2022c), Z. Zhang et al. (2021, 2022b), and Castaneda (2022) covering steel sheet sheathed shear walls, connections and shear wall modeling, and floors/diaphragms, respectively.

A 10-story CFS-framed building is currently under construction for subsequent testing on the newly upgraded 6-DOF Large High-Performance Outdoor Shake Table Facility (LHPOST6) at the NHERI@UC San Diego Experimental Facility (Van Den Einde et al. 2021). The seismic testing is scheduled to begin in spring 2025. This capstone experimental program (colloquially known as CFS10 – see [cfs10.ucsd.edu](https://cfs10.ucsd.edu)) will provide an opportunity to assess seismic structural and non-structural performance for a unique class of buildings and will conclude with live fire testing. Key features of this tall structure is the inclusion of complete architectural finishes and a building height that exceeds the current height restrictions outlined in U.S. design standards (ASCE/SEI 2016, 2022). The experiments will yield critical full-scale, system-level benchmark data for a state-of-the-art CFS building subjected to multi-directional seismic forces, contributing to advancements in structural and non-structural seismic design codes and performance-based guidance. Additionally, complementary live fire tests conducted by Cal Poly San Luis Obispo will provide valuable insights into thermal behavior and smoke spread within earthquake-damaged compartments.

The 10-story test building was designed as a CFS-framed structure situated at a hypothetical site in a seismically active region near Irvine, California, characterized by a Site Class C condition (very dense soil and soft rock) as detailed in Singh et al. (2022a). The test building features CFS steel studs, shear walls sheathed with sheet steel on one side, and gravity walls. The tested building is taken as a slice from a larger archetype. Thus, the north face of the test building is exterior and includes an EIFS finish, all other faces are interior finishes. The floors utilize a dry system (no

poured concrete) and are constructed using ledger-framed CFS joists topped with cementitious (dry) structural panels assembled in volumetric or floor modules. The lateral force-resisting system employs Type I shear walls with single-sided steel sheet sheathing. Many of the shear wall details are beyond current AISI S400 provisions, including the use of HSS sections for chord studs in lower floors, Power-Actuated Fasteners (PAFs) for connections between steel sheet and HSS chord studs, and steel sheet fasteners (PAFs or screws) utilizing spacings that are outside of AISI S400 design tables. Tension in shear wall chords is handled by tie-rods in one principal direction of the building and directly connected tension chord studs using splice plates in the other direction. The building was designed to a total height of 30.5 m (100 ft), exceeding the 19.8 m (65 ft) height limitation imposed by ASCE 7-16 (ASCE/SEI 2016) and ASCE 7-22 (ASCE/SEI 2022). Its estimated effective seismic weight,  $W$ , is 1575.0 kN (354.1 kips), and the design seismic base shear force,  $V$ , was calculated as 173.2 kN (38.9 kips) in both orthogonal directions assuming an  $R=6.5$  and a site selected in Irvine, California. Singh et al. (2022a) provides a detailed structural design narrative for the test building, while Singh et al. (2024) offers additional updates to the specimen design, including integration of an operable (stair) egress system, with drift-release connections, shake table attachments, and an expansion of construction methods (modular and panelized construction details). Figure 1b presents a 3D rendering of the CFS-NHERI test structure atop LHPOST6.

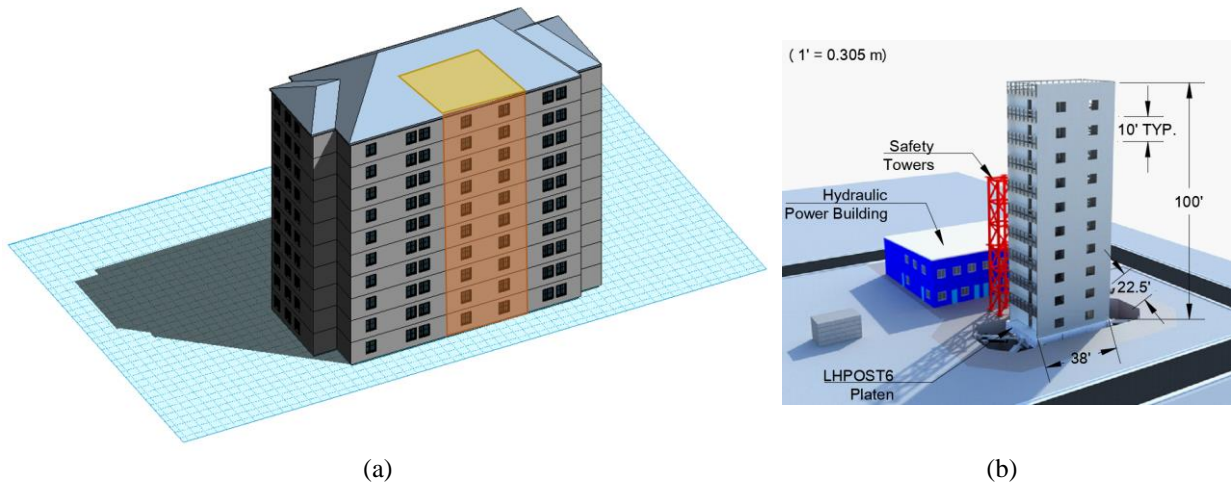


Figure 1: 3D rendering view of (a) The 10-story Archetype full Building and (b) the CFS-NHERI 10-story test structure atop LHPOST6 (J. Zhang et al. 2024)

To predict the response of the test building, two distinct numerical models have been employed. The first model (J. Zhang et al. 2024), developed using the OpenSeesPy framework (McKenna et al. 2000; Zhu et al. 2018), is a design-level phenomenological-based model. The term "design-level" is used here to denote a model that is intentionally simplified and low in degrees of freedom (DOF), focusing primarily on capturing the key structural features that significantly influence the seismic response of the building. This simplification enables the model to perform numerous analysis runs efficiently on a standard desktop computer, typically completing within a day. The design-level finite element (FE) model is built using a methodology described by Singh et al. (2024), which was applied to simulate the response of a full-scale, six-story cold-formed steel (CFS) building subjected to unidirectional shaking (Hutchinson et al. 2021). Singh et al. (2024) model has been rigorously evaluated and compared with prior experimental data, showing good

agreement. A comprehensive description of the design-level model is available in J. Zhang et al. (2024).

The second model, the primary focus of this paper, is a higher-fidelity model compared to the design-level model mentioned above. In this approach, individual elements are used to represent each structural component, including studs, tracks, sheathings, hold-downs, and tie rods. The model incorporates a wide range of geometric nonlinearities, such as buckling of steel sheets as well as local, distortional, and global buckling of CFS members. Compared to the design-level phenomenological-based model, this model is expected to require significantly longer analysis time. The outputs from this model were validated against component-level test data and subsequently compared with the results obtained from the simplified design-level model of the building-system.

## **2. Description and Validation of the developed higher-fidelity model**

Previous studies on modeling the dynamic behavior of CFS-framed structures have primarily relied on simplifications to reduce computational demands. Commonly, shear walls are represented using either a nonlinear spring or two diagonal nonlinear braces (Shamim and Rogers 2012). Gravity systems are typically excluded, except for a leaning P- $\Delta$  column, and diaphragms are often assumed to be fully rigid, modeled with a single element. Leng et al. (2017) introduced higher-fidelity models for the two-story CFS-NEES test building, enabling more precise predictions of the performance of individual CFS-framed components under seismic loading. These models allowed for detailed analysis of load path redistribution to elements such as chord studs, tracks, and sheathing that form shear wall lines.

Building on this, Z. Zhang et al. (2022c) constructed a high-fidelity model to study the lateral behavior of CFS-framed wall lines, incorporating steel sheet-sheathed shear walls, gravity walls, and the influence of non-structural finishes. Compared to simplified models, the high-fidelity approaches by Leng et al. (2017) and Z. Zhang et al. (2022c) demonstrated significantly improved accuracy in predicting the seismic response of CFS-framed buildings and wall lines, respectively. In the present study, the high-fidelity modeling strategies outlined by Leng et al. (2017) and Z. Zhang et al. (2022c) are adopted. This higher-fidelity model enables deeper insights into load path redistribution along wall lines and among components of shear walls (SW) and gravity walls (GW), including chord studs, tracks, and sheathing.

### *2.1 Model Description*

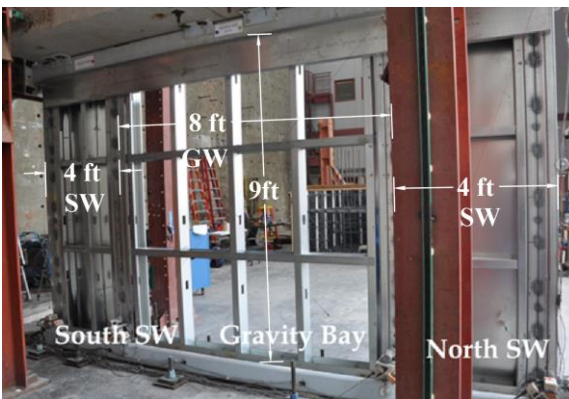
Using the OpenSeesPy framework (McKenna et al. 2000; Zhu et al. 2018), a high-fidelity finite element model is developed. To illustrate the modeling approach, the finite element model of the test specimen SGGS-1HD from the wall-line dynamic testing program by Singh et al. (2022b, 2022c) is employed as an example (see Figure 2a). In this model, displacement-based beam-column line elements are used to represent all framing members, including studs and tracks, as shown in Figure 2b. The "section aggregator" command is utilized to separately define axial and flexural responses for these beam-column elements.

An elastic-perfectly plastic (EPP) material model, scaled to reflect actual nominal capacities, is used to simulate the nonlinear axial and flexural behavior of tracks and field studs. The maximum strength of these elements is calculated based on AISI S100-16 (AISI 2016), which accounts for

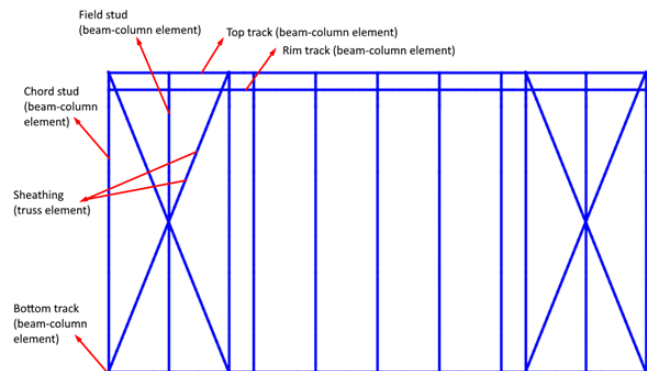
local buckling, distortional buckling, and yielding (as explained in detail in Section 2.2). For chord studs, a more advanced nonlinear material model is adopted. Specifically, the Pinching4 material model (Figure 3) from the OpenSeesPy library is used to capture local and distortional buckling behavior. This material model incorporates a detailed four-point backbone curve and accounts for stiffness degradation during unloading, reloading, and strength reduction, as outlined in Section 9.8 of ASCE 41-17 (ASCE/SEI 2017).

While centerline definitions are used for most elements, exceptions are made for ledger (rim) tracks and end joints. For these components, the full web height is modeled using additional beam elements, oriented perpendicular and rigidly connected to the horizontal beam-column elements representing the ledger tracks or end-joists. This approach allows moment transfer across the entire depth of the ledger or end-joist, rather than at a single-point joint, resulting in a more accurate representation of moment distribution between studs and ledger-track/end-joist connections.

The steel sheet sheathing, shown in Figure 2a, is represented utilizing two diagonal truss elements (Figure 2b), using a Pinching4 material model (Figure 3). The parameters for this model are calibrated using cyclic test results from a CFS-framed shear wall with steel sheathing, specifically specimen CW2 from Rizk and Rogers (2017). This specimen was selected due to its similar configuration to the SGGS-1HD wall-line test, including comparable framing and sheathing thicknesses as well as fastener spacing. The material model also accounts for the height difference between the CW2 specimen (2.44 m or 8 ft) and the SGGS-1HD wall-line (2.74 m or 9 ft). For walls incorporating nonstructural finishes, additional diagonal truss elements are introduced, and also modeled using the Pinching4 hysteretic material. The parameters for the gypsum finish are derived from cyclic test data on CFS-framed walls clad with gypsum boards, as documented by Morello (2009). This approach aims to more accurately represent the sheathing and nonstructural finish behavior under cyclic loading conditions.



(a)



(b)



(c)

Figure 2: (a) Test specimen SGGs-1HD tested by Singh et al. (2022b, 2022c); (b) OpenSeesPy numerical model of SGGs-1HD wall-line specimen; (c) Shear buckling waves in the steel sheet sheathing (Singh et al. 2021)

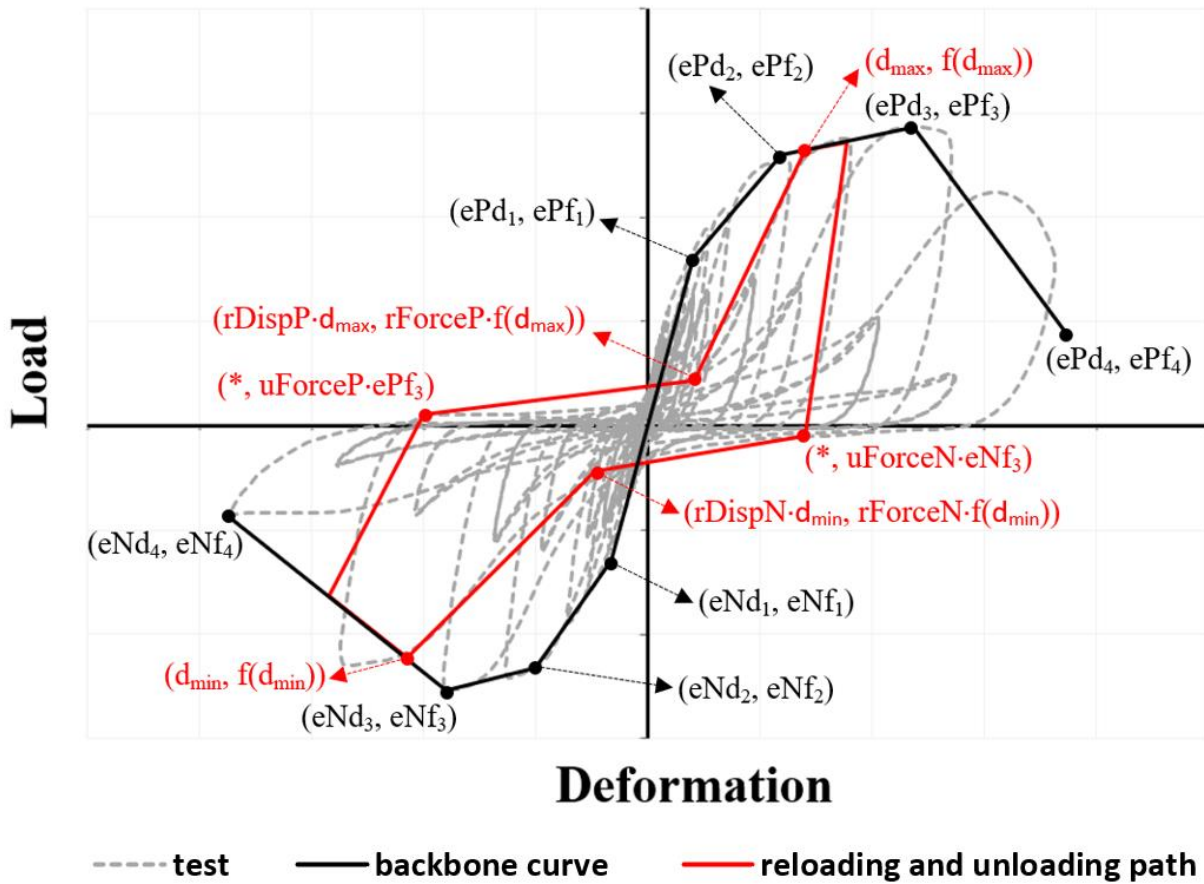


Figure 3: Equivalent energy Pinching 4 fit to an experimental response

## 2.2 Stability Assumptions

Buckling of CFS framing members has been consistently observed in recent experimental studies on CFS-framed shear walls, wall lines, and building-level tests (Schafer et al. 2016; Brière & Rogers 2018; Rizk & Rogers 2018; Santos & Rogers 2018; Singh et al. 2021). Consequently, it is essential to incorporate buckling strength limits of framing members into the modeling of CFS-framed buildings and their subsystems. In this study (as mentioned earlier), studs and tracks are represented using displacement-based beam-column elements with displacement formulations (Mazzoni et al. 2006).

The model employs a corotational coordinate transformation, which is well-suited for problems involving large displacements-small strains. To account for global flexural buckling behavior, individual framing members are discretized into multiple beam-column elements and analyzed within a geometrically nonlinear framework. The section aggregator command (Mazzoni et al. 2006) is utilized to combine uniaxial material models that represent axial, flexural, and torsional behaviors into a single beam-column element section. These uniaxial material models are treated independently.

Axial, in-plane flexural, and out-of-plane flexural behaviors are incorporated into the 3D beam-column elements used in the model. The uniaxial material models and their associated properties for framing members under axial loading are detailed in Table 1, while those for members under in-plane bending are summarized in Table 2. Similarly, Table 3 outlines the uniaxial material models and properties for members subjected to out-of-plane bending. For HSS chord studs, AISC 360 specifications (AISC 2022) were employed to determine material parameters.

For both axial and flexural behaviors, the material model's yield strength is replaced with the nominal strength of the member, accounting for limitations imposed by yielding and various buckling modes. This approach ensures that all components are constrained to their nominal capacities, explicitly incorporating local and distortional buckling of cross-sections as well as yielding. Global flexural buckling is directly modeled within the finite element framework itself. Further details regarding this approach can be found in Z. Zhang's Ph.D. thesis (Zhang 2023).

In design, the stability coefficient  $\theta$  (ASCE/SEI 2022) may be utilized to approximately assess the extent to which P- $\Delta$  effects can significantly amplify moments and displacements. In modeling, this is handled directly through consideration of geometric nonlinearity (i.e. iterative solutions that satisfy equilibrium in the deformed configuration). It is possible to also model without considering geometric nonlinearity – and this is conducted here and reported in a later section, to assess the importance of story-level P- $\Delta$  effects, as associated with  $\theta$ , in the frame.

Table 1: Uniaxial material model properties for each framing member subjected to axial load

| Member       | Material Model | Axial Stiffness | Tensile Peak Strength | Compressive Peak Strength                    |
|--------------|----------------|-----------------|-----------------------|--|
| Chord Stud   | EPP            | $EA_e$          | $T_n$                 | $P_n^\# = P_{nlo}$                           |
| Gravity Stud | EPP            | $EA_e$          | $T_n$                 | $P_n^* = P_{nlo}$ or $\min(P_{nlo}, P_{nd})$ |
| Track        | EPP            | $EA_e$          | $T_n$                 | $P_n^* = P_{nlo}$                            |
| Header Track | EPP            | $EA_e$          | $T_n$                 | $P_n^* = P_{nlo}$                            |
| Ledger Track | EPP            | $EA_e$          | $T_n$                 | $P_n^\# = \min(P_{nlo}, P_{nd})$             |

- Notes: 1.  $P_n^\#$  values can be referenced from AISI D100 (AISI 2017a), stud local buckling strength  $P_{nlo}$  can be found in Table III-2, stud distortional buckling strength  $P_{nd}$  can be found in Table III-5, and ledger track  $P_{nlo}$  is in Table III-3, otherwise, adopt the Direct Strength Method (DSM) in Section E of AISI S100-16 (AISI 2016). For HSS studs, AISC 360 is utilized for the nominal capacity.
2.  $A_e$  means the effective area under axial compression, while  $A$  implies the gross section area.
3. If gravity studs are sheathed, then the nominal axial compressive strength is limited by local buckling. However, if it unsheathed, the nominal axial compressive strength is controlled by the smaller value between local buckling and distortional buckling nominal strength values.
4. If the chord stud or header track are built-up sections, simply add up the single section stiffness and strength values to obtain the built-up section properties.
5. The yielding strength of the EPP material model is replaced with member nominal strength as limited by yielding and various buckling behaviors.

Table 2: Uniaxial material model properties for each framing member subjected to in-plane bending

| Member       | Material Model | Bending Stiffness | Positive Peak Strength | Negative Peak Material |
|--------------|----------------|-------------------|------------------------|------------------------|
| Chord Stud   | Pinching4      | $EI_y$            | $M_{nyc}^\#$           | $M_{nyt}^\#$           |
| Gravity Stud | EPP            | $EI_y$            | $M_{nyc}^*$            | $M_{nyt}^*$            |
| Track        | EPP            | $EI_y$            | $M_{nyc}^*$            | $M_{nyt}^*$            |
| Header Track | EPP            | $EI_y$            | $M_{nyc}^*$            | $M_{nyt}^*$            |
| Ledger Track | EPP            | $EI_x$            | $M_{nx}^*$             | $M_{nx}^*$             |

- Notes: 1.  $M_n^\#$  can be referenced from ASCE41 (ASCE/SEI 2017), and  $M_n^*$  needs to employ the Direct Strength Method (DSM) in Section F of AISI S100-16 (AISI 2016). For HSS studs, AISC 360 is utilized.
2. Subscript x refers to major axis bending, while y implies weak axis bending.
3.  $M_{nyc}$  and  $M_{nyt}$  refer to the weak axis bending nominal strength corresponding to the web in tension and compression, respectively.
4. If the chord stud or header track are built-up sections, simply add up the single section stiffness and strength values to obtain the built-up section properties.
5. The yielding strength of the EPP material model is replaced with member nominal strength as limited by yielding and various buckling behaviors.

Table 3: Uniaxial material model properties for each framing member subjected to out-of-plane bending

| Member       | Material Model | Bending Stiffness | Positive Peak Strength | Negative Peak Material |
|--------------|----------------|-------------------|------------------------|------------------------|
| Chord Stud   | EPP            | $EI_{xe}$         | $M_{nx}^\#$            | $M_{nx}^\#$            |
| Gravity Stud | EPP            | $EI_{xe}$         | $M_{nx}^\#$            | $M_{nx}^\#$            |
| Track        | EPP            | $EI_{xe}$         | $M_{nx}^*$             | $M_{nx}^*$             |
| Header Track | EPP            | $EI_{xe}$         | $M_{nx}^*$             | $M_{nx}^*$             |
| Ledger Track | EPP            | $EI_y$            | $M_{nyc}^*$            | $M_{nyt}^*$            |

- Notes: 1.  $M_n^\#$  can be determined by the nominal strength limited by local buckling in Table II-2 or the nominal strength limited by distortional buckling in Table II-8 of AISI D100 (AISI 2017a).  $M_n^*$  needs to employ the Direct Strength Method (DSM) in Section F of AISI S100-16 (AISI 2016); For HSS studs AISC 360 is utilized.
2. Subscript x refers to major axis bending, while y implies weak axis bending.
3.  $M_{nyt}$  and  $M_{nyc}$  refer to the weak axis bending nominal strength corresponding to the web in tension and compression, respectively.
4.  $I_{xe}$  means the effective moment of inertia about the major axis, which can be referenced from Table II-2 in AISI D100 (AISI 2017a). For HSS sections AISC 360 is utilized.
5. If the chord stud or header track are built-up sections, simply add up the single section stiffness and strength values to obtain the built-up section properties.
6. The yielding strength of the EPP material model is replaced with member nominal strength as limited by yielding and various buckling behaviors.

### 2.3 Model Validation

The performance of the developed finite element modeling protocol is assessed by comparing its predictions with experimental data from the SGGS-1HD wall-line test (Singh et al. 2021). As demonstrated in Figure 4, there is acceptable agreement between the predicted and observed cyclic responses. Additionally, Figures 5a and 5b present the axial force and bending moment diagrams for the wall line, derived from the finite element model. While the properties of the diagonal truss elements representing the performance of the steel sheet shear wall are experimentally derived, the bending behavior captured in Figure 5b is unique to the wall line configuration and an important contributor to the observed final performance.

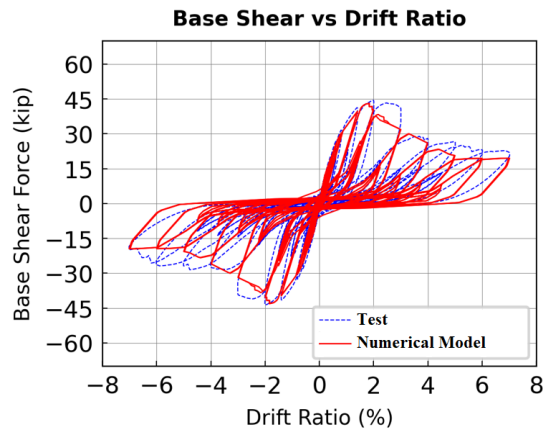


Figure 4: Experimental and FE base-shear vs. drift ratio response (specimen SGGS-1HD)

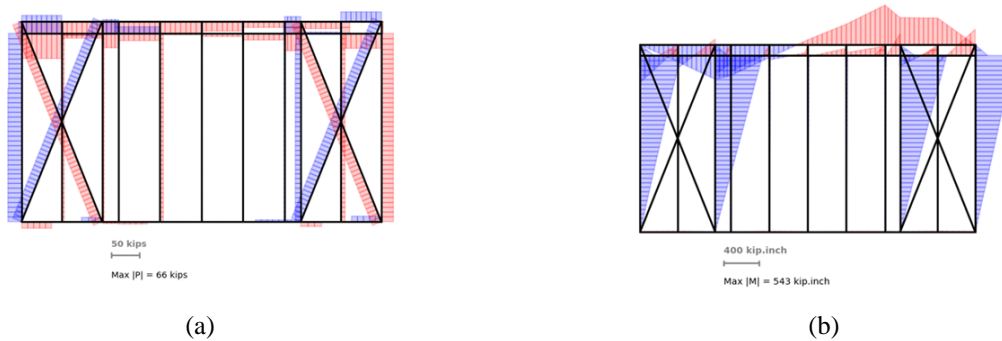


Figure 5: Numerical (a) axial force diagram and (b) bending moment diagram of SGGS-1HD (at maximum absolute load)- In the diagrams, blue and red are used to represent positive and negative forces and moments, respectively

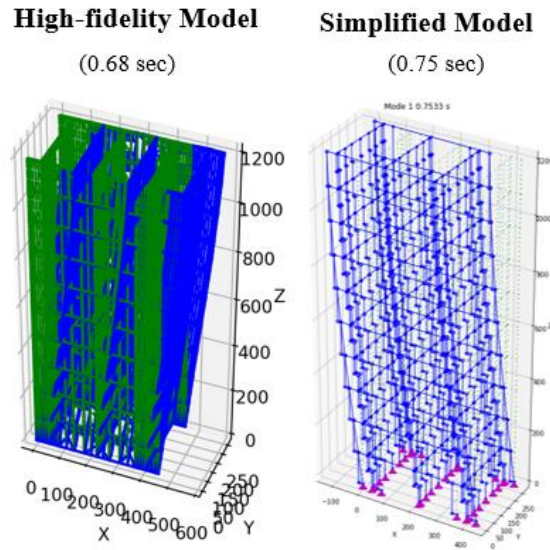
## 3. Comparison between the results of high-fidelity and simplified models

In this section, the simplified design-level phenomenological-based model created by J. Zhang et al. (Zhang et al. 2024) and the higher-fidelity model are each utilized and compared while conducting pre-test analysis of the 10-story CFS archetype building. Example results for both free vibration and time history analyses are considered in the comparison.

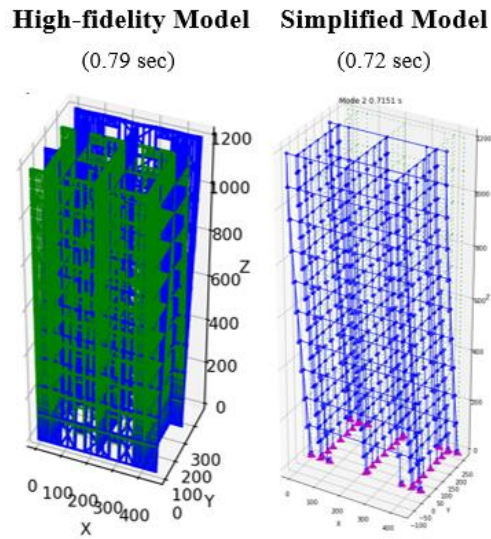
### 3.1 Free Vibration Analysis Results

Eigenvalue analysis is used to compute the natural frequencies and mode shapes of the 10-story CFS building considering each of the modeling approaches. Free vibration results comparison, shown in Figure 6, demonstrate that the first three time periods of the simplified design-level model

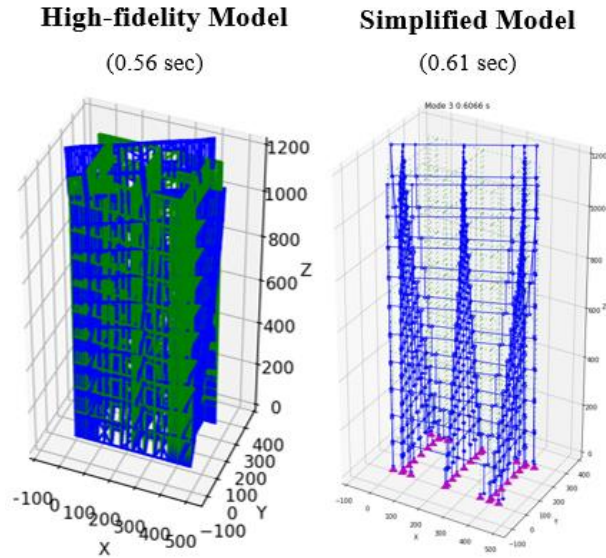
and the high-fidelity model are comparable. In both models, the first natural mode shape is identified as the E-W (X) direction translation, the second mode is N-S (Y) direction translation, and the third mode is a torsional mode. A similar level of agreement in the two models is observed in the higher-order modes as well.



(a) E-W (X) direction



(b) N-S (Y) direction



(c) Torsional

Figure 6: Comparison of the first three mode shapes in both models of the 10-story CFS building specimen

### 3.2 Time History Analysis Results

In this section, the results of both numerical models of the test building subjected to a bi-directional (XY)  $MCE_R$  scaled motion from the 1994 Northridge earthquake, notably the Canoga Park - Topanga Can motion are compared.  $MCE_R$  refers to the risk-targeted *maximum considered earthquake* response level at which the ground motion is applied. It is also noted that in the following, the motion is applied at an orientation of  $90^\circ$  relative to the original recording orientation. For all ground motions considered during the planning phase of the capstone test motion pairs are considered at both  $0^\circ$  and  $90^\circ$  orientations.

Figures 7 and 8 illustrate the roof acceleration time history in the X (E-W) and Y (N-S) directions, respectively, as predicted by the high-fidelity model. As observed in the figures, the peak roof acceleration in the X direction exceeds  $1.35g$ , which is approximately 25% higher than the peak roof acceleration in the Y direction. On the other hand, Figure 9 presents the total roof drift ratio time history in both directions, also predicted by the high-fidelity model. Once again, the X direction (E-W) experienced a higher peak roof interstory drift ratio compared to the Y direction (N-S), reaching a maximum of 0.52%. A comparison of the base-shear versus drift ratio responses predicted by the simplified design-level model and the higher-fidelity model in both directions, as shown in Figure 10, reveals good agreement between the two models. Key parameters such as initial stiffness, maximum base shear, and maximum drift ratio are also comparable. As shown in Figure 11, the Peak Interstory Drift Ratio (PIDR) profile of both models is in good agreement in both directions, except for some discrepancies in the higher stories in the Y direction. Similarly, the Peak Floor Acceleration (PFA) profiles predicted by both models in both directions are in good agreement, as illustrated in Figure 12. It is noted that future investigations will compare the response of both models across a broader suite of earthquake motions in preparation for motion selection for use in shake table testing.

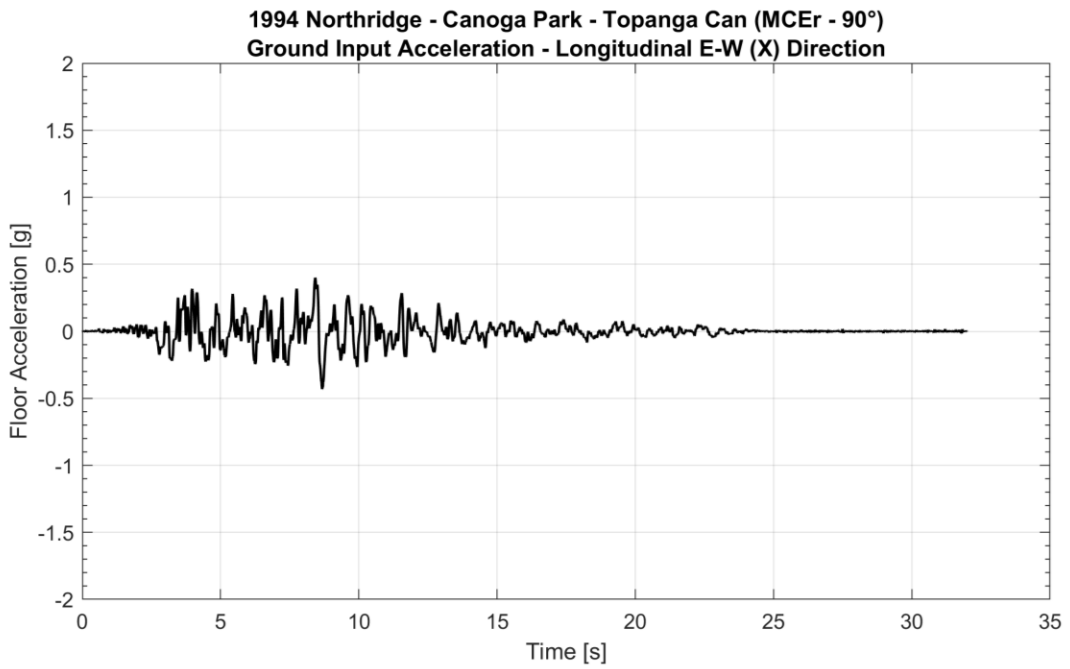
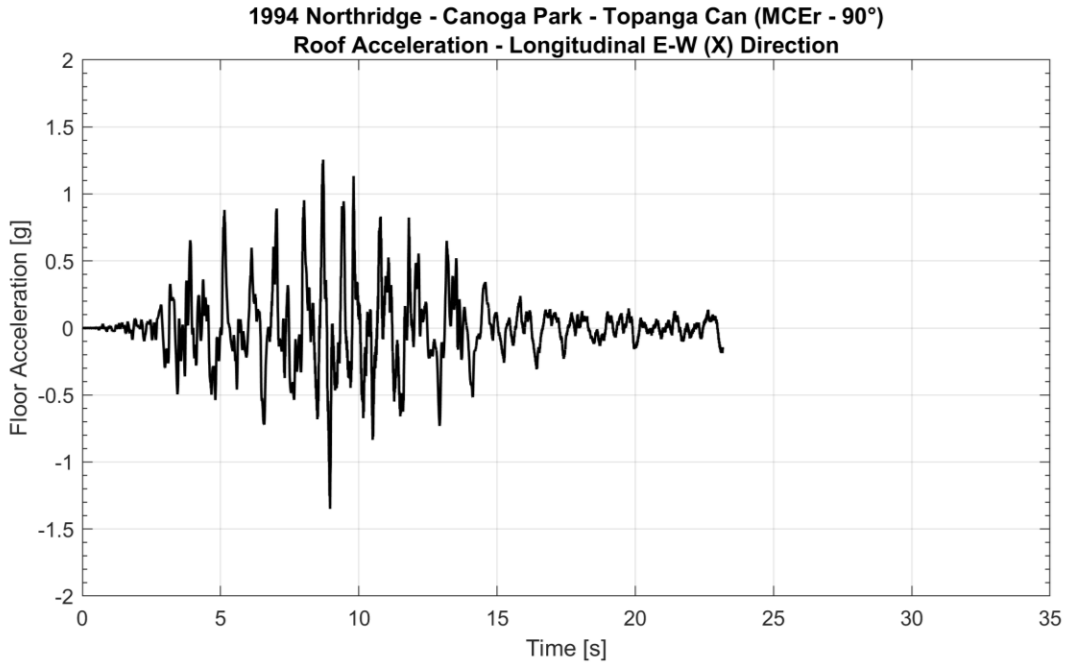


Figure 7: Roof Acceleration Time History (predicted by the high-fidelity model) and ground input acceleration in X direction (1994 Northridge - Canoga Park - Topanga Can (MCE<sub>R</sub> - 90°)) – Note: The simulation was intentionally terminated early, more than 10 seconds beyond the peak response

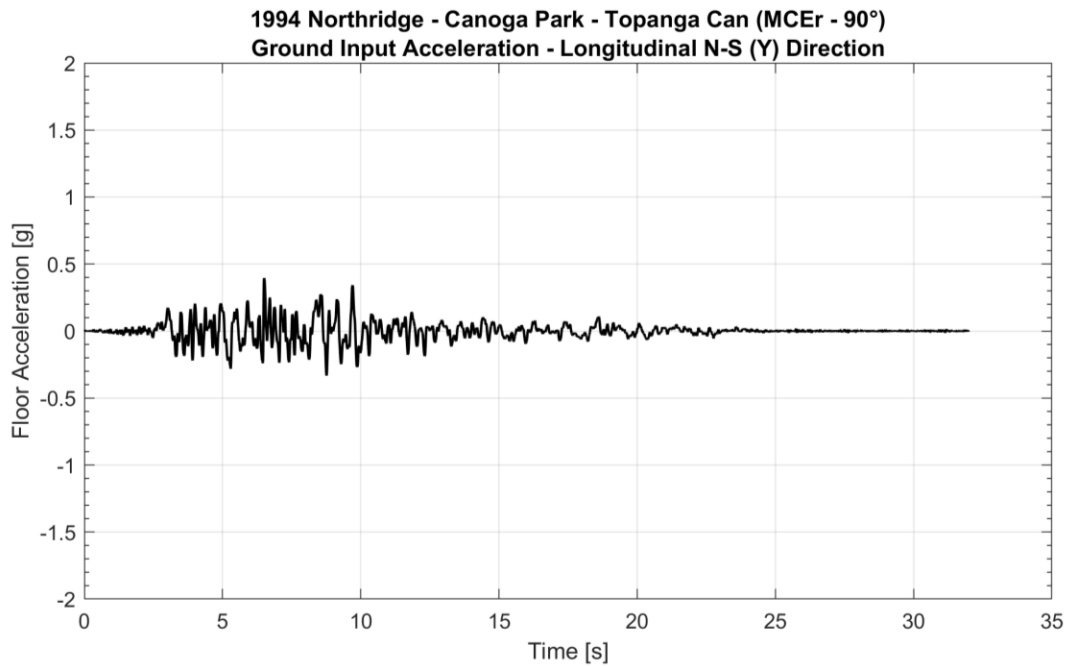
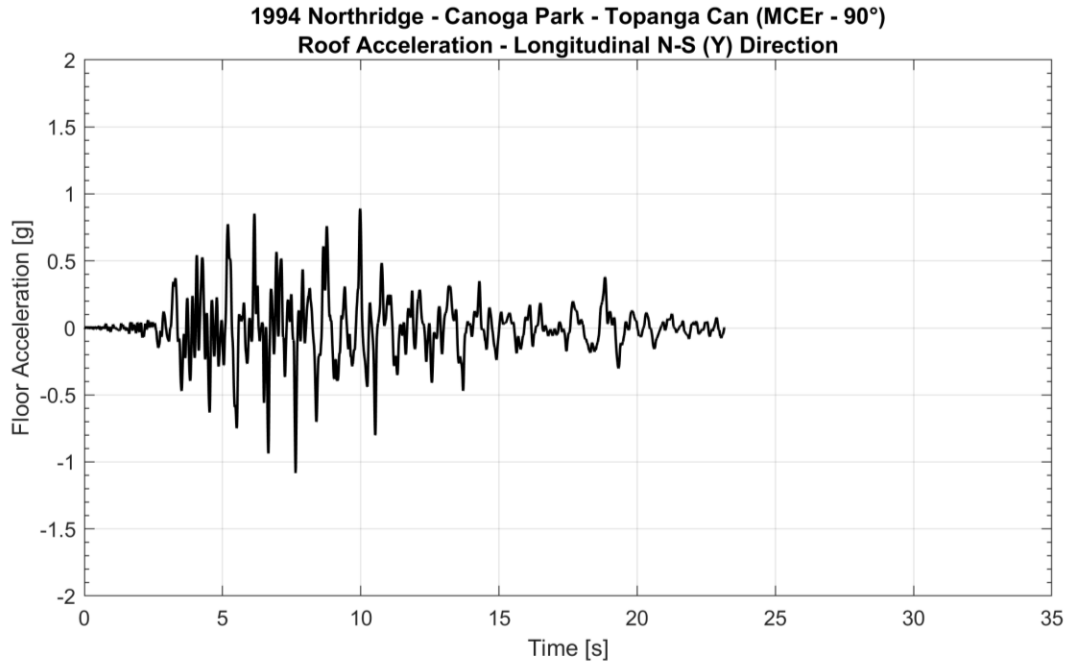


Figure 8: Roof Acceleration Time History (predicted by the high-fidelity model) and ground input acceleration in Y direction (1994 Northridge - Canoga Park - Topanga Can (MCE<sub>R</sub> - 90°)) – Note: The simulation was intentionally terminated early, more than 10 seconds beyond the peak response

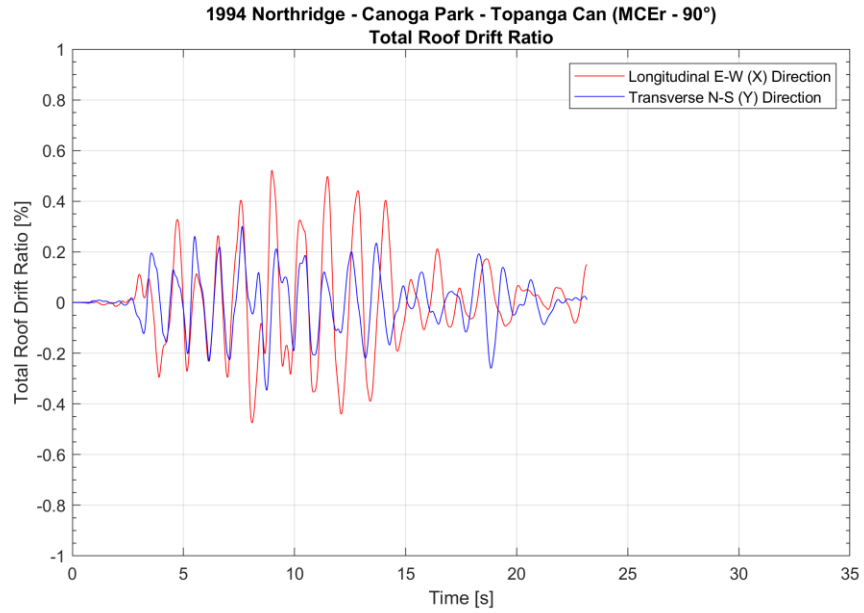


Figure 9: Total Roof Drift Ratio Time History (predicted by the high-fidelity model) in both directions (1994 Northridge - Canoga Park - Topanga Can ( $MCE_R - 90^\circ$ ))

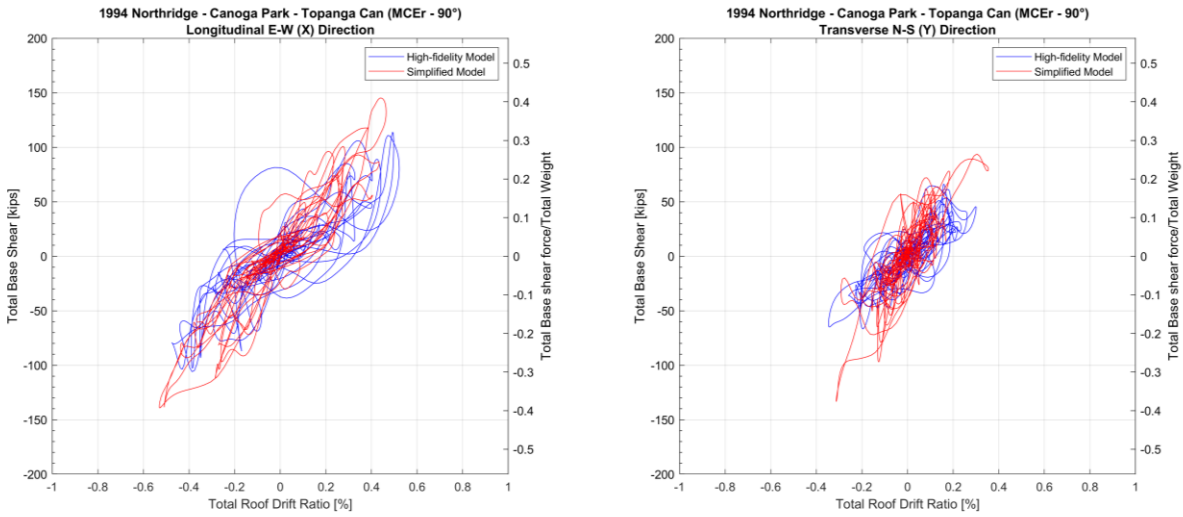


Figure 10: Comparison of Base-Shear vs. Roof Drift Ratio responses predicted by the simplified design-level model and the high-fidelity model in both directions (1994 Northridge - Canoga Park - Topanga Can ( $MCE_R - 90^\circ$ ))

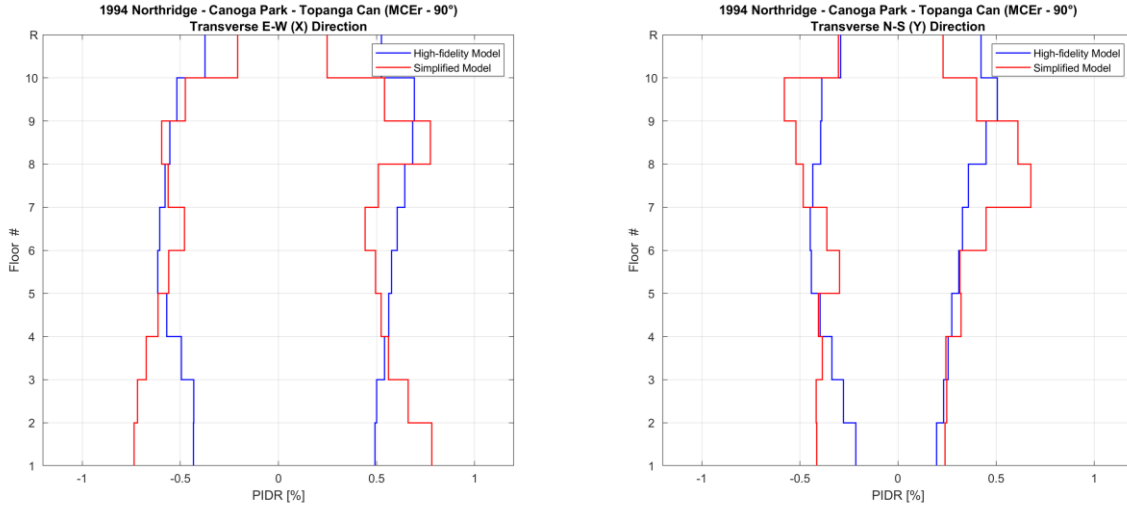


Figure 11: Comparison of Peak Interstory Drift Ratio (PIDR) Profiles predicted by the simplified design-level model and the high-fidelity model in both directions (1994 Northridge - Canoga Park - Topanga Can (MCE<sub>R</sub> - 90°))

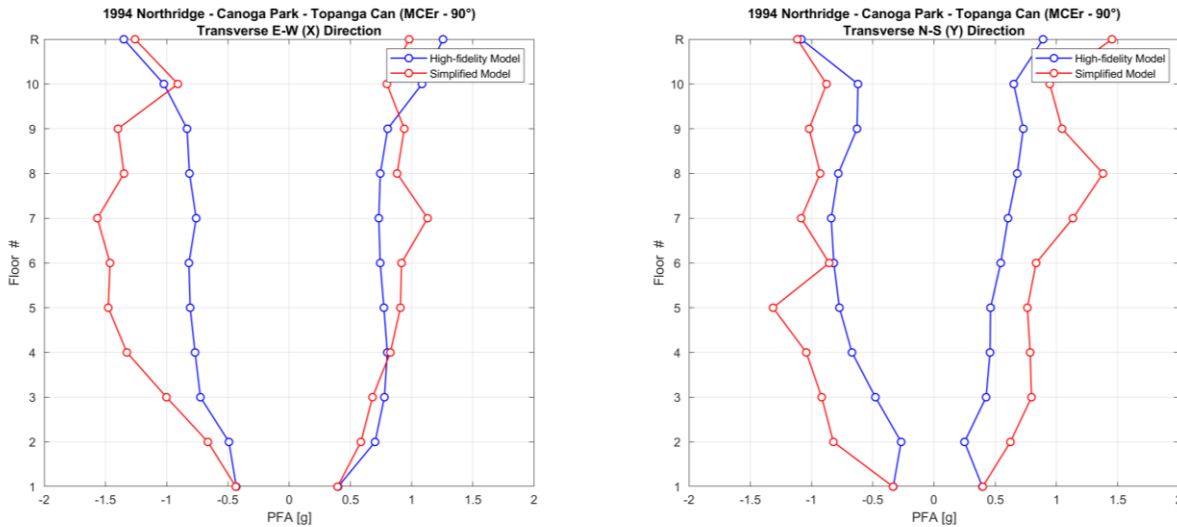


Figure 12: Comparison of Peak Floor Acceleration (PFA) Profiles predicted by the simplified design-level model and the high-fidelity model in both directions (1994 Northridge - Canoga Park - Topanga Can (MCE<sub>R</sub> - 90°))

To examine the influence of the geometric nonlinearity (transformation type), Linear, PDelta, and Corotational transformations as available in the OpenSeesPy library (Mazzoni et al. 2006) were utilized, and the resulting outcomes were compared under the 1994 Northridge - Canoga Park - Topanga Can (MCE<sub>R</sub> - 0°) excitation. As shown in Figure 13, there is no significant difference in the base shear versus drift ratio curves among the three studied transformations. The PIDR profiles predicted by the three models are also very similar, as seen in Figure 14. Though a partial study, these results suggest that second-order deformations do not significantly influence the outcomes, at least at the observed drift level. Instead, the observed nonlinearity appears to be primarily governed by the Pinching4 model rather than by P-Delta effects. However, it is important to note that these findings are based on a single motion, and different motions may yield different outcomes, warranting further investigation. The research team is currently conducting this extended analysis, and the findings will be presented in future publications.

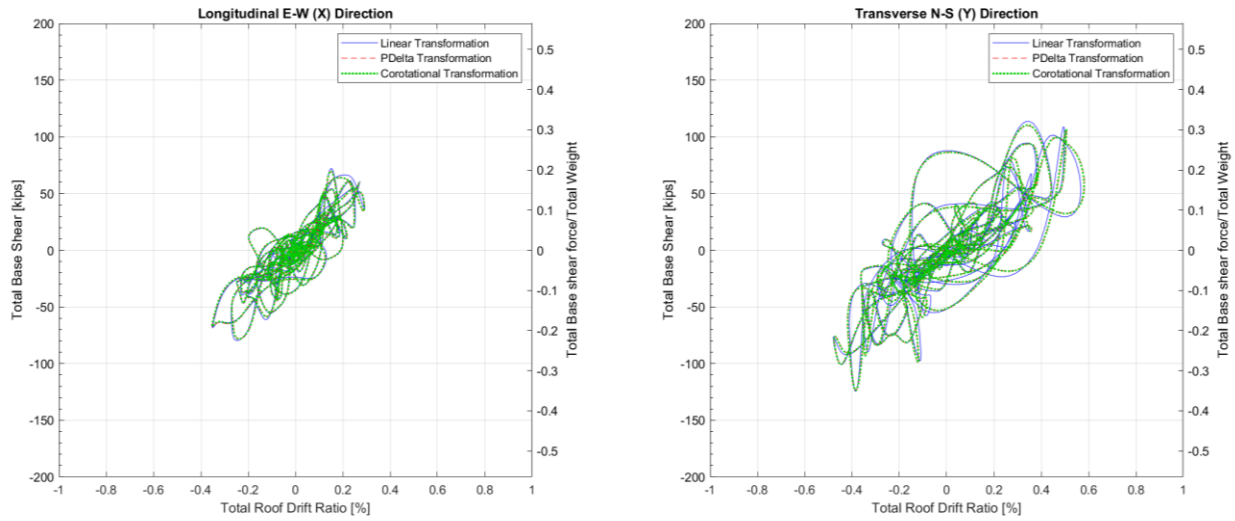


Figure 13: Comparison of Base-Shear vs. Drift Ratio responses predicted by the high-fidelity model in both directions using three different geometric transformation types (1994 Northridge - Canoga Park - Topanga Can (MCE<sub>R</sub> - 0°))

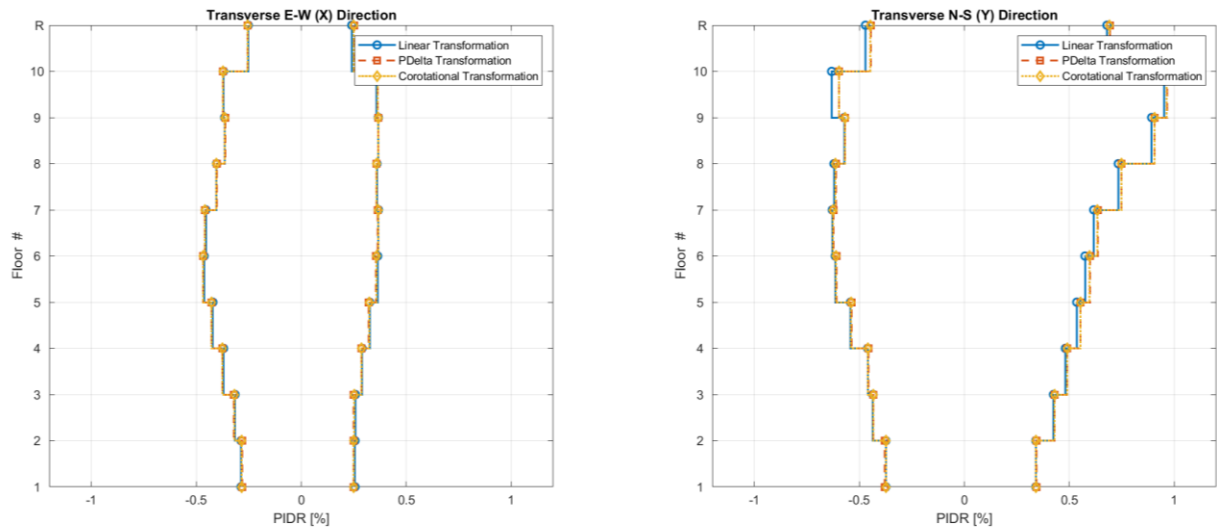


Figure 14: Comparison of PIDR Profiles predicted by the high-fidelity model in both directions using three different geometric transformation types (1994 Northridge - Canoga Park - Topanga Can (MCE<sub>R</sub> - 0°))

#### 4. Conclusions

This research focuses on the role of stability assumptions in the numerical modeling of cold-formed steel (CFS) structures under seismic loads. A high-fidelity finite element model developed in OpenSeesPy was thoroughly described, with a focus on how local, distortional, and global buckling of CFS members, and shear buckling of steel sheet shear walls, are incorporated into the model. Validation against experimental data for a CFS-framed wall line demonstrates the model's ability to accurately capture the complex cyclic behavior of CFS-framed wall systems. A 10-story CFS building archetype (slice) is then modeled using the high-fidelity FEM approach and an independently developed simplified design-level FEM. Comparison amongst the two models

including eigenvalue analysis and overlays of base-shear versus drift ratio responses, peak interstory drift ratios profiles, and peak floor acceleration profiles was made. The comparisons revealed good agreement between the two approaches for the studied  $MCE_R$ -scaled earthquake motion. The similarity in results among the studied geometric transformation types suggests that second-order deformations have minimal influence at the observed drift levels, with nonlinear behavior primarily controlled by the Pinching4 model rather than P-Delta effects. This research provides valuable insights for developing strategies to incorporate stability limits into seismic modeling practices for CFS-framed buildings, fostering more accurate analysis and broader practical application of these systems.

## Acknowledgments

The research presented in this paper is funded through the National Science Foundation (NSF), USA grants CMMI 1663569 and CMMI 1663348, project entitled: Collaborative Research: Seismic Resiliency of Repetitively Framed Mid-Rise Cold-Formed Steel Buildings. Findings, opinions, and conclusions are those of the authors and do not necessarily reflect those of the sponsoring organizations.

## References

- AISC (2022). "Specification for Structural Steel Buildings, AISC 360-22." American Institute of Steel Construction, Chicago, IL, USA.
- AISI (2015a). "North American Specification for Cold-Formed Steel Structural Framing, AISI S240-15." American Iron and Steel Institute, Washington, D.C., USA.
- AISI (2015b). "North American Specification for Seismic Design of Cold-Formed Steel Structural Systems, AISI S400-15." American Iron and Steel Institute, Washington, D.C., USA.
- AISI (2016). "North American Specification for the Design of Cold-Formed Steel Structural Members, AISI S100-16." American Iron and Steel Institute, Washington, D.C., USA.
- AISI (2017a). "Cold-formed steel design manual." American Iron and Steel Institute (AISI).
- ASCE/SEI (2016). "Minimum Design Loads and Associated Criteria for Buildings and Other Structures, ASCE/SEI 7-16." American Society of Civil Engineers, Reston, VA, USA.
- ASCE/SEI (2017). "Seismic Evaluation and Retrofit of Existing Buildings, ASCE/SEI 41-17." American Society of Civil Engineers, Reston, VA, USA.
- ASCE/SEI (2022). "Minimum Design Loads and Associated Criteria for Buildings and Other Structures, ASCE/SEI 7-22." American Society of Civil Engineers, Reston, VA, USA.
- Brière, V., Rogers, C. A. (2018). "Higher capacity cold-formed steel sheathed and framed shear walls for mid-rise buildings: Part 2 [Research Report]." Dept. of Civil Engineering and Applied Mechanics, McGill University.
- Castaneda, H. (2022). "Seismic performance of cold-formed steel diaphragms." Ph.D. thesis. University of Massachusetts, Amherst, Amherst, MA, USA.
- Hutchinson, T. C., Wang, X., Hegemier, G., Kamath, P., Meacham, B. (2021). "Earthquake and postearthquake fire testing of a midrise cold-formed steel-framed building. I: Building response and physical damage." *Journal of Structural Engineering*, 147(9): 04021125. DOI: [https://doi.org/10.1061/\(ASCE\)ST.1943-541X.00030](https://doi.org/10.1061/(ASCE)ST.1943-541X.00030).
- Leng, J., Peterman, K. D., Bian, G., Buonopane, S. G., Schafer, B. W. (2017). "Modeling seismic response of a full-scale cold-formed steel-framed building." *Engineering Structures*, 153: 146-165. DOI: <https://doi.org/10.1016/j.engstruct.2017.10.008>.
- Mazzoni, S., McKenna, F., Scott, M. H., Fenves, G. L. (2006). "OpenSees command language manual." Pacific Earthquake Engineering Research (PEER) Center. (pp. 137–158).
- McKenna, F., Fenves, G. L., Scott, M. H. (2000). "Open System for Earthquake Engineering Simulation." University of California, Berkeley. <http://opensees.berkeley.edu>.
- Morello, D. (2009). "Seismic performance of multi-storey structures with cold-formed steel wood sheathed shear walls." Master Thesis. Department of Civil Engineering and Applied Mechanics, McGill University, Montreal, Canada.
- Peterman, K. D., Stehman, M. J. J., Madsen, R. L., Buonopane, S. G., Nakata, N., Schafer, B. W. (2016). "Experimental seismic response of a full-scale cold-formed steel-framed building. I: System-level response."

- Journal of Structural Engineering*, 142(12): 04016127. DOI: [https://doi.org/10.1061/\(ASCE\)ST.1943-541X.0001577](https://doi.org/10.1061/(ASCE)ST.1943-541X.0001577).
- Rizk, R., Rogers, C. A. (2017). "Higher strength cold-formed steel framed steel shear walls for mid-rise construction." Research Report, Department of Civil Engineering and Applied Mechanics, McGill University, Montreal, Canada.
- Rizk, R., Rogers, C. A. (2018). "Higher strength cold-formed steel framed/steel shear walls for mid-rise construction." Research Report, Department of Civil Engineering and Applied Mechanics, McGill University, Montreal, Canada.
- Santos, V., Rogers, C. A. (2018). "Higher capacity cold-formed steel sheathed and framed shear walls for mid-rise buildings: Part 1 [Research Report]." Dept. of Civil Engineering and Applied Mechanics, McGill University.
- Schafer, B. W., Ayhan, D., Leng, J., Liu, P., Padilla-Llano, D., Peterman, K. D., Stehman, M., Buonopane, S. G., Eatherton, M., Madsen, R., Manley, B., Moen, C. D., Nakata, N., Rogers, C., Yu, C. (2016). "Seismic Response and Engineering of Cold-formed Steel Framed Buildings." *Structures*, 8, 197–212. DOI: <https://doi.org/10.1016/j.istruc.2016.05.009>.
- Shamim, I., Rogers, C. A. (2012). "Numerical modeling and calibration of CFS framed shear walls under dynamic loading." *Proceedings of the 21st International Specialty Conference on Cold-Formed Steel Structures*, St. Louis, MO, USA.
- Singh, A. (2023). "Seismic Behavior of Cold-Formed Steel-Framed Wall-Line Systems in Mid-Rise Buildings." Doctoral dissertation. University of California San Diego, La Jolla, CA.
- Singh, A., Wang, X., Hutchinson, T. C. (2021). "Lateral Response of Cold-Formed Steel Framed Steel Sheathed In-line Wall Systems Detailed for Mid-Rise Buildings. Part I: Shake Table Test Phase (Structural Systems Research Project Report Rep. No. SSRP-19/05)." Department of Structural Engineering, University of California San Diego.
- Singh, A., Hutchinson, T. C., Torabian, S., Schafer, B. W., Peterman, K. D., Padgett, L., Jones, H. (2022a). "Structural design narrative of the CFS-NHERI 10-story test building for multi-dimensional shake table testing." *Proceedings of the Cold-Formed Steel Research Consortium Colloquium 2022*, Baltimore, MD, USA.
- Singh, A., Hutchinson, T. C., Wang, X., Zhang, Z., Schafer, B. W., Derveni, F., Castaneda, H., Peterman, K. D. (2022b). "Steel Sheet Sheathed Cold-formed Steel Framed In-line Wall Systems. I: Impact of Structural Detailing." *Journal of Structural Engineering*, 148(12): 04022193. DOI: [https://doi.org/10.1061/\(ASCE\)ST.1943-541X.0003433](https://doi.org/10.1061/(ASCE)ST.1943-541X.0003433).
- Singh, A., Hutchinson, T. C., Wang, X., Zhang, Z., Schafer, B. W., Derveni, F., Castaneda, H., Peterman, K. D. (2022c). "Steel Sheet Sheathed Cold-Formed Steel Framed In-line Wall Systems. II: Impact of Nonstructural Detailing." *Journal of Structural Engineering*, 148(12): 04022194. DOI: [https://doi.org/10.1061/\(ASCE\)ST.1943-541X.0003434](https://doi.org/10.1061/(ASCE)ST.1943-541X.0003434).
- Singh, A., Zhang, J., Eladly, M., Jones, H., Kovac, A., Padgett, L., Rivera, D., Smith, K., Torabian, S., Peterman, K., Schafer, B., Hutchinson, T. (2024). "CFS-NHERI 10-Story Building Shake Table Test Specimen: Design Updates." *Proceedings of the 18th World Conference on Earthquake Engineering (WCEE2024)*, Milan, Italy, June 30–July 5, 2024.
- Singh, A., Zhang, Z., Wang, X., Schafer, B.W., Hutchinson, T.C. (2024). "Practice-oriented numerical model for seismic response of cold-formed steel-framed mid-rise buildings." *Engineering Structures*, 319: 118833. DOI: <https://doi.org/10.1016/j.engstruct.2024.118833>.
- Van Den Einde, L., Conte, J. P., Restrepo, J. I., Bustamante, R., Halvorson, M., Hutchinson, T. C., Lai, C.-T., Lotfizadeh, K., Luco, J. E., Morrison, M. L., Mosqueda, G., Nemeth, M., Ozelik, O., Restrepo, S., Rodriguez, A., Shing, P. B., Thoen, B., Tsampras, G. (2021). "NHERI@UC San Diego 6-DOF large high-performance outdoor shake table facility." *Frontiers in Built Environment*, 6. DOI: <https://doi.org/10.3389/fbuil.2020.580333>.
- Zhang, J., Singh, A., Eladly, M., Schafer, B. W., Hutchinson, T. C. (2024). "Pre-Test Numerical Modeling of the CFS-NHERI 10-Story Capstone Building." *Proceedings of the 18th World Conference on Earthquake Engineering (WCEE2024)*, Milan, Italy, June 30–July 5, 2024.
- Zhang, Z., Singh, A., Dervani, F., Torabian, S., Peterman, K. D., Hutchinson, T. C., Schafer, B. W. (2021). "Cyclic experiments on isolated steel sheet connections for CFS framed steel sheet sheathed shear walls with new configurations." *Engineering Structures*, 244: 112805. DOI: <https://doi.org/10.1016/j.engstruct.2021.112805>.
- Zhang, Z., Singh, A., Dervani, F., Torabian, S., Peterman, K. D., Hutchinson, T. C., Schafer, B. W. (2022b). "Cyclic experiments on steel sheet connections for standard CFS framed steel sheet sheathed shear walls." *Journal of Structural Engineering*, 148(2): 04021261. DOI: [https://doi.org/10.1061/\(ASCE\)ST.1943-541X.000323](https://doi.org/10.1061/(ASCE)ST.1943-541X.000323).
- Zhang, Z., Speicher, M. S., Singh, A., Hutchinson, T. C., Schafer, B. W. (2022c). "Effects of Modeling Decisions on the Lateral Performance of Cold-Formed Steel Framed Walls." *Proceedings of the Cold-Formed Steel Research Consortium Colloquium 2022*, Baltimore, MD, USA.

Zhang, Z. (2023). "Simulation and Performance of Steel Sheet Sheathed Shear Walls in CFS-Framed Building Systems." Doctoral dissertation. Johns Hopkins University, Baltimore, MD, USA.

Zhu, M., McKenna, F., Scott, M. H. (2018). "OpenSeesPy: Python library for the OpenSees finite element framework." *Software X*, 7: 6-11. DOI: <https://doi.org/10.1016/j.softx.2017.10.009>.